Iron Oxide Tube-in-Tube Nanostructures

Chun-Jiang Jia,[†] Ling-Dong Sun,*[,†] Zheng-Guang Yan,[†] Yu-Cheng Pang,[†] Li-Ping You,[‡] and Chun-Hua Yan*[,†]

Beijing National Laboratory for Molecular Sciences, State Key Laboratory of Rare Earth Materials Chemistry and Applications & PKU-HKU Joint Laboratory in Rare Earth Materials and Bioinorganic Chemistry, and Electron Microscopy Laboratory, Peking University, Beijing 100871, China

Received: May 18, 2007; In Final Form: June 26, 2007

Single-crystalline hematite tube-in-tube nanostructures were prepared by a facile one-step hydrothermal method. The structure, shape, and formation mechanism of the tube-in-tube nanostructures were investigated. The results disclosed that the hematite tube-in-tube nanostructures were formed through a multisite dissolution process of the ellipsoid precursors. What is more, the tube-in-tube nanostructure is a single crystal in nature, and a simple combination of a small tube filling into a big one can be excluded. Single-crystalline magnetite and maghemite tube-in-tube nanostructures were also obtained via a simple reduction or reduction and reoxidation process with the hematite as the precursor. The facile and mild reaction route could be useful for the fabrication of complex tubular nanostructures.

Introduction

Nanotubes have attracted much attention since the discovery of carbon nanotubes in 1991[1] because of their great importance in both scientific research and technological applications. Besides the synthesis of various nanotubes,[2−4] the fabrication of complex or composite tubular nanostructures has attracted extensive interest due to their novel properties and advantages in constructing nanodevices. The different forms of composite one-dimensional nanostructures including coaxial nanocables[5] and coaxial nanotubes[6] have been prepared by physical methods, such as laser ablation[5] and thermal evaporation.[6] Recently, there have been reports on the fabrication of carbon "tube-in-tube" nanostructures through a two-step soft chemical process,[7,8] while the synthesis of a single-crystalline tube-in-tube nanostructure of inorganic materials by a one-step solution method has not been reported.

Iron oxides are very important functional materials due to their wide applications in information storage, catalysis, gas sensors, and so on. Various iron oxide nanostructures including monodispersed nanoparticles,[9−13] nanowires,[14−16] nanobelts,[14,15] and nanotubes,[17−19] etc.,[20−22] have been reported. Here, we report a facile synthesis of single-crystalline iron oxide tube-in-tube nanostructures by a simple one-step hydrothermal method. The structure, morphology, and formation mechanism of the tube-in-tube nanostructure were investigated.

Experimental Section

Preparations. *Hematite Tube-in-Tube Nanostructures.* The hematite tube-in-tube nanostructures were synthesized through the hydrothermal treatment of mixed $FeCl_3$, $NH_4H_2PO_4$, and Na_2SO_4 solutions. In a typical experimental procedure, 3.20 mL of $FeCl_3$ (0.5 mol·L^{-1}), 0.90 mL $NH_4H_2PO_4$ (0.04 mol·L^{-1}), and 1.10 mL of Na_2SO_4 (0.04 mol·L^{-1}) aqueous solution were mixed with vigorous stirring. Distilled water was added to keep the final volume to 80 mL, so the final concentrations of $FeCl_3$, $NH_4H_2PO_4$, and Na_2SO_4 were 0.02, 4.5×10^{-4}, and 5.5×10^{-4} mol·L^{-1}, respectively. After being stirred for 20 min, the mixture was transferred into a Teflon-lined stainless steel autoclave with a capacity of 100 mL for hydrothermal treatment at 220 °C for 48 h. As the autoclave cooled to room temperature naturally, the precipitates were separated by centrifugation, washed with distilled water and absolute ethanol, and dried under vacuum at 80 °C.

Magnetite and Maghemite Tube-in-Tube Nanostructures. Magnetite tube-in-tube nanostructures were prepared via a reduction process with the corresponding hematite products as precursors. Under a continuous hydrogen/argon [$H_2/(H_2 + Ar) = 8/100$] gas flow, the dried hematite powders were annealed in a tube furnace at 360 °C for 5 h and cooled to room temperature naturally. The obtained black powders were magnetite products. Maghemite tube-in-tube nanostructures were obtained by oxidation of the above as-prepared magnetite powders exposed in air at 240 °C for 2 h.

Characterizations. The powder X-ray diffraction (XRD) patterns were recorded on a Rigaku D/MAX-2000 diffractometer using Cu Kα radiation ($\lambda = 1.5418$ Å). Scanning electron microscopy (SEM) images were obtained with the DB-235 focused ion beam (FIB) system. Transmission electron microscopy (TEM), high-resolution TEM (HRTEM), scanning transmission electron microscopy (STEM), and energy-dispersive X-ray (EDX) spectroscopy were performed with a Philips Tecnai F30 FEG-TEM instrument operated at 300 kV and a JEOL 2010F TEM instrument operated at 200 kV. Raman spectra were determined on a Horiba Jobin Yvon LabRam HR 800 spectrometer equipped with a grating of 1800 grooves/mm, an Olympus BX41 microscope (100× objective lens), and a charge-coupled device detector. The spectra were measured with the 488 nm line of an Ar^+ laser; a backscattering geometry was adopted for the measurement with a laser power of 0.03 mW. The magnetic properties were investigated on a Quantum Design

* To whom correspondence should be addressed. Fax: +86-10-6275-4179. (C.-H. Yan) E-mail: yan@pku.edu.cn. (L.-D. Sun) E-mail: sun@pku.edu.cn.

[†] Beijing National Laboratory for Molecular Sciences, State Key Laboratory of Rare Earth Materials Chemistry and Applications & PKU-HKU Joint Laboratory in Rare Earth Materials and Bioinorganic Chemistry.

[‡] Electron Microscopy Laboratory.

10.1021/jp073837q CCC: $37.00
Published on Web 08/10/2007

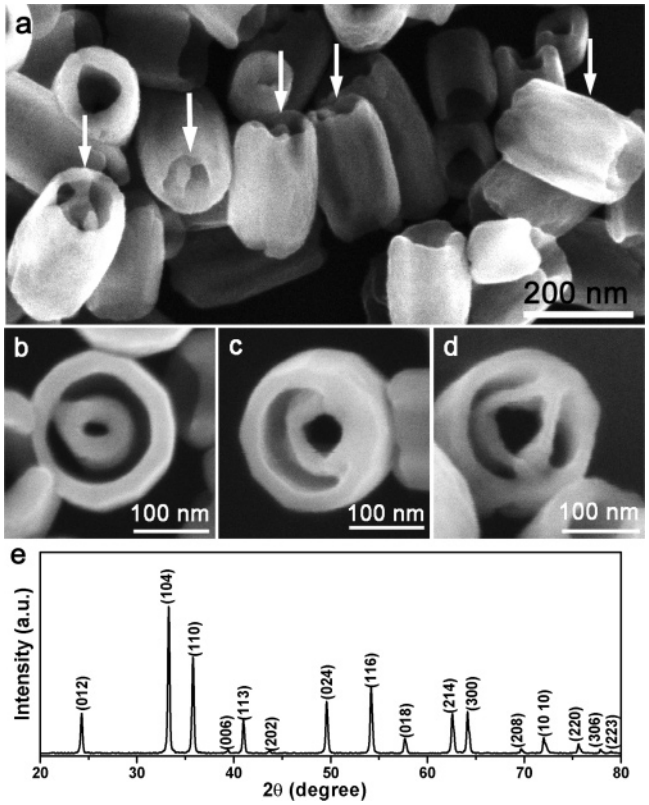

Figure 1. (a) SEM image of the as-synthesized hematite products. The observed tube-in-tube nanostructures are marked with arrows. (b−d) top-view SEM images of the single tube-in-tube nanostructures showing morphological diversity. (e) XRD patterns of the as-synthesized hematite products.

MPMS XL-5 (SQUID) magnetometer. The samples were put in a low-susceptibility plastic sample holder for measurements. The diamagnetic contribution from the sample holder was carefully determined and subsequently subtracted.

Results and Discussion

The morphology of the products is characterized with scanning electron microscopy. A careful inspection reveals that there are two kinds of products of hematite (Figure 1a and Figure S1, Supporting Information). One is a tube with a single solid wall, while the other is a tube with double walls. Actually, the latter one is a tube-in-tube nanostructure consisting of two subtubes (inner and outer ones). It is evident that the walls of the single tube-in-tube nanostructure are partially connected (Figure 1b−d), which is distinct from the reported composite coaxial nanotubes, whose adjacent tube walls are fully connected.[6] The XRD pattern of the product is shown in Figure 1e. All of the diffraction peaks are well indexed to a pure corundum structure of hematite (JCPDS 33-664), indicating that both the inner and outer tubes of the tube-in-tube nanostructure are hematite, which was also confirmed by the following TEM investigations.

The detailed structural information on the tube-in-tube nanostructures is investigated with transmission electron microscopy. The selected area electron diffraction (SAED) pattern (inset of Figure 2a) shows that the tube-in-tube nanostructure (Figure 2a) is a single crystallite nanostructure growing along the [001] direction (*c*-axis of hematite). Figure 2b shows the STEM image of the same tube-in-tube nanostructure collected with a high-angle annular dark field (HADDF) detector, in which both the inner and outer subtube walls are brighter than the other parts, due to the relatively large number of atoms. The compositional line profiles of this tube-in-tube nanostructure probed with EDX spectroscopy exhibit well-correlated iron and oxygen signals across the inner and outer tube walls, which is highly consistent with the STEM image. EDX spectra acquired from different sites across the tube are shown in Figure S2, Supporting Information.

Figure 2c shows a tube-in-tube nanostructure viewed from the top. The SAED pattern (inset of Figure 2c) indicates that this tube-in-tube nanostructure is also a single crystal with an axis direction of [001], consistent with the results of Figure 2a. The HRTEM image (Figure 2d) of one part of the tube-in-tube nanostructure shows the well-segregated inner and outer tube walls, while the lattice images of the tube walls exhibit completely the same periodicity. For another part of the tube-in-tube nanostructure (Figure 2e), the inner and outer tube walls are still connected. The continuous lattice images across the inner and outer walls are clearly observed, showing the same periodicity as that in Figure 2d,f, indicating that the connection part with light contrast is an inherent part of the tube-in-tube nanostructure but does not fill subsequently. The lattice fringes of all three parts are highly consistent with the structure of hematite projected along [001] (inset of Figure 2f). TEM and HRTEM information on another tube-in-tube nanostructure observed from the side view (Figure S3, Supporting Information) also confirms that the tube-in-tube nanostructure is not a simple combination of two individual nanotubes, but a single crystal.

Besides the structural analysis on the tube-in-tube nanostructure, the formation mechanism is also investigated. We have reported the formation of hematite nanotubes through the dissolution of spindle-like precursors with the mediation of phosphate ions.[19] In this work, the coupled mediation of phosphate and sulfate ions induces the formation of two kinds of precursors, a large amount of spindles and a few ellipsoids (marked by a white ellipse in Figure 3a). The crystal face dependent adsorption selectivities of phosphate and sulfate ions on hematite are almost the same, and they both prefer to adsorb on the prismatic faces of hematite, such as {110} and {100}, other than the basal face {001},[10] but the absolute adsorption ability of sulfate is much weaker than that of phosphate,[10] which is confirmed by the morphology of the products with the presence of phosphate or sulfate ions as the additives, respectively. Polyhedron nanoparticles were obtained with the sulfate ions as additives, while spindles growing along [001] were formed with the mediation of phosphate ions (see Figure S4, Supporting Information). Also a small amount of phosphate ions coexisting with sulfate ions will induce the formation of hematite spindle precursors along [001], as well as an ellipsoid with weakened growth along the *c*-axis. For the spindle precursors, their relatively sharp tips can easily be attacked by the protons in acidic solutions, inducing the dissolution to start from the tips and proceed along the longitude (*c*-axis of the hematite). During this process, the side surfaces of the spindle are protected by the adsorption of phosphate and sulfate ions.[19] Therefore, conventionally single-walled nanotubes growing along [001] (Figure S5, Supporting Information) are formed, similar to the formation of hematite nanotubes we reported.[17] However, for the ellipsoid-like precursors, their relatively flat tops make it possible for the dissolution to happen not only at the centered tips, but also at several high-energy sites on the top simultaneously, which is confirmed by the intermediates with multiconcave sites on the tops (marked by a white ellipse in Figure 3b). In the magnified SEM images (Figure 3c,d), nanostructures with one centered hole and a few surrounding holes coexisting

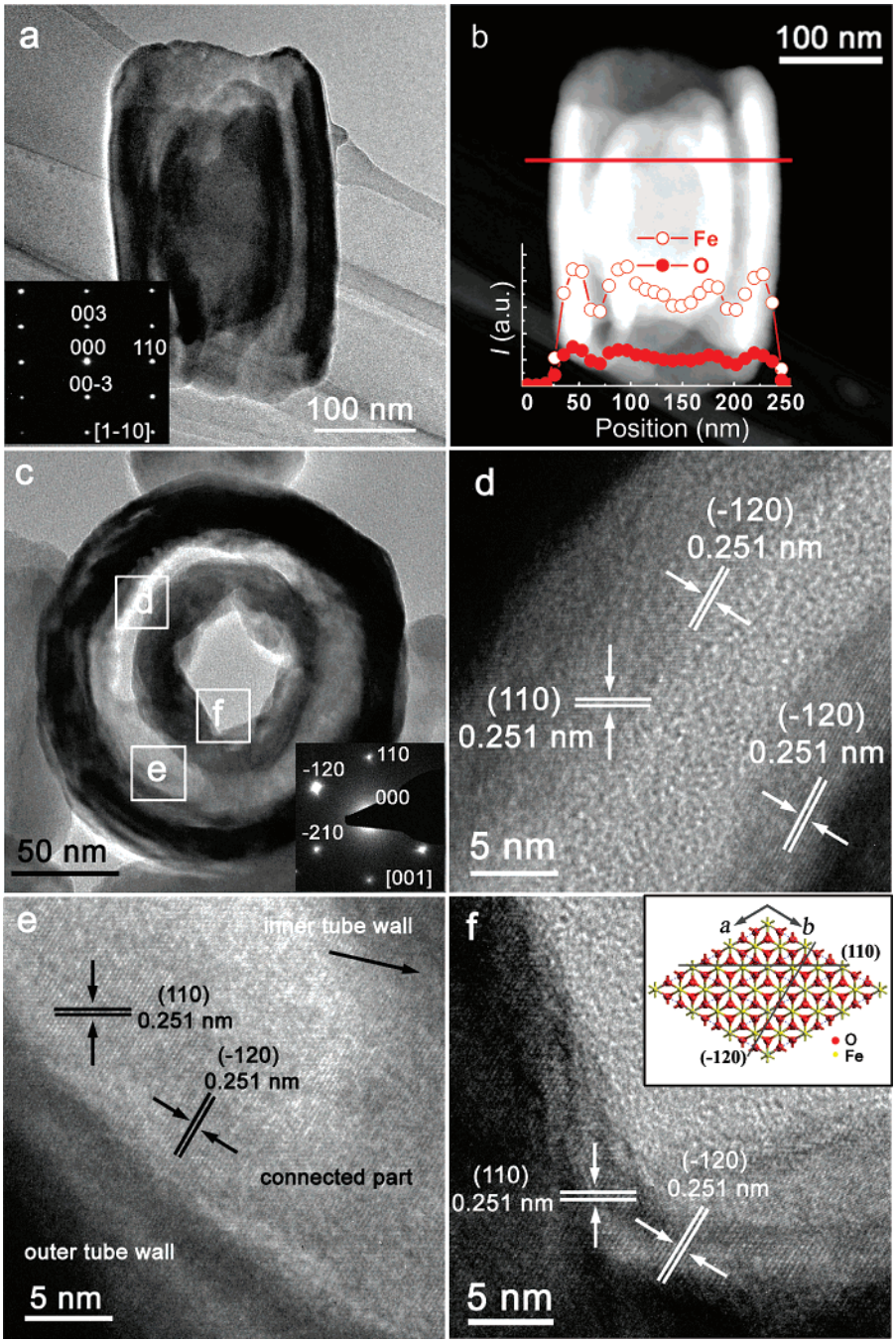

Figure 2. (a) Side-view TEM image of a single tube-in-tube nanostructure and the SAED pattern. (b) STEM image and compositional line profiles across the tube-in-tube nanostructure probed by EDX spectroscopy scanning along the red line. (c) TEM image and SAED pattern of a tube-in-tube nanostructure viewed from the top. (d−f) HRTEM images of the tube walls as marked with the white frame in (c).

on the tops of the ellipsoid-like particles can be evidently identified. With an increase of the reaction time, the neighboring holes could merge together into a continuous one, similar to the formation of the ordinary single-walled hematite nanotubes. The side surfaces of the inner and outer tubes are protected due to the adsorption of phosphate and sulfate ions, and tube-in-tube nanostructures are formed in the end. Because of the randomly distributed high-energy sites on the top of the ellipsoids, the multisite dissolution process and the morphology of the final tube-in-tube nanostructures exhibit interesting diversity, as illustrated in Scheme 1 and Figure 1a−d. An important aspect that should be stressed is that, with the optimized ratio of sulfate to phosphate ions, not all of the precursors are present as ellipsoids and the diversity of the succedent dissolution makes it hard to obtain products dominated by tube-in-tube structures.

Interestingly, the inner and outer subtube walls of the observed tube-in-tube nanostructures are all partly connected. It is just the connection that prevents the displacement of the inner tubes, which ensures the single-crystal nature of the tube-in-tube nanostructures. Although the tube-in-tube structure cannot be obtained with high purity, the "multisite dissolution" approach provides a new strategy to fabricate single-crystal complex tubular nanostructures through soft chemical techniques. Through the double-additive (phosphate and sulfate ions) mediation route, other interesting iron oxide nanostructures, such as single-crystal nanorings and porous nanotubes, could also be prepared.

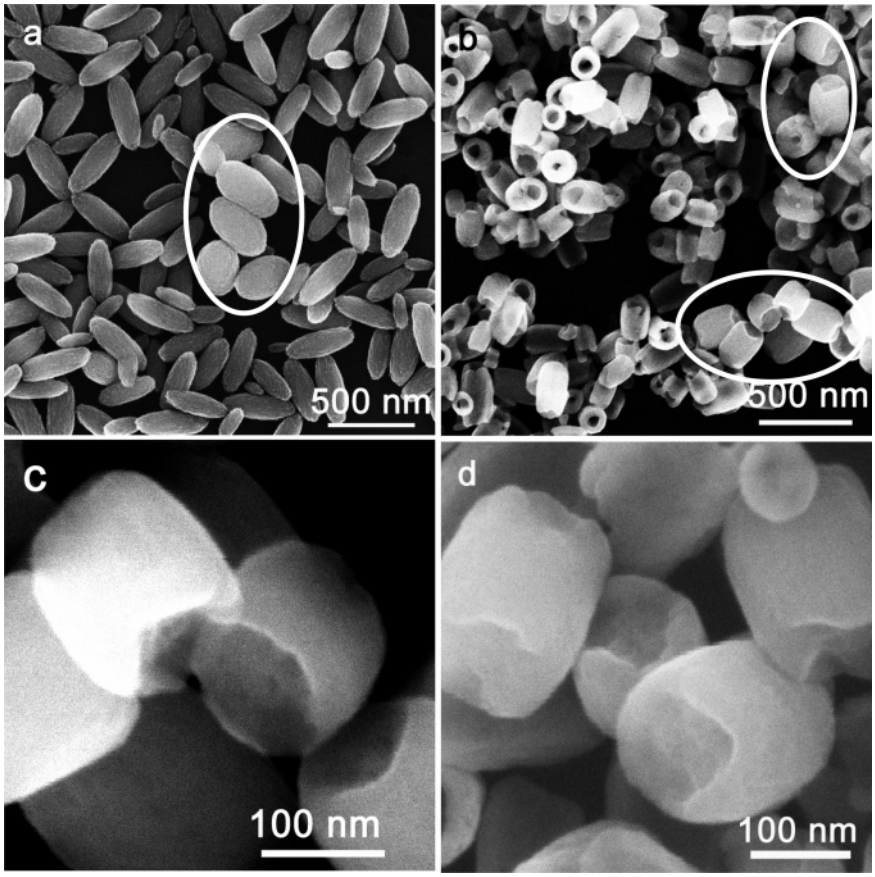

Figure 3. SEM images of the hematite products prepared with reaction times of 1 h (a) and 24 h (b−d).

SCHEME 1: Schematic Illustrations (Top View) of the Formation Process of Hematite Tube-in-Tube Nanostructures with Diversity

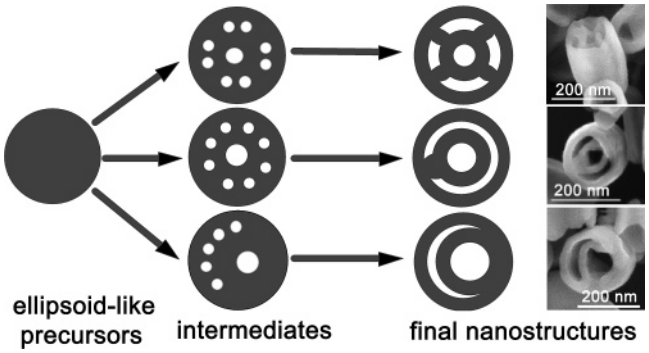

Hematite is an antiferromagnet that undergoes a spin-flip transition at the Morin temperature (T_M); the bulk value of T_M is 263 K. As an important magnetic material, the magnetism of hematite is always being studied. Here, the magnetic behaviors of hematite nanostructures (composed of nanotubes and tube-in-tube nanostructures) shown in Figures 1 and S1 were investigated using a commercial superconducting quantum interference device (SQUID) magnetometer. The zero-field cooling (ZFC) and field cooling (FC) behavior is shown in Figure S6a, Supporting Information, and T_M is 210 K, which is much lower that of the bulk, but a little higher than that of the pure nanotubes[19] (200 K, Figure S7a, Supporting Information). The coercive force (H_c) at 300 K is 180 Oe (Figure S6b) for hematite nanostructures composed of nanotubes and tube-in-tube nanostructures; this value is lower than that of pure nanotubes[19] (350 Oe, Figure S7b). The variation of T_M and H_c for different nanostructures may result from their difference in microstructure such as lattice strain and defects caused by a decrease of the crystallite size and an increase of surface area.[23−25]

Moreover, magnetite (Fe_3O_4) and maghemite (γ-Fe_2O_3) tube-in-tube nanostructures were prepared through a reduction or reduction and reoxidation process with hematite as the precursor. Parts a and b of Figure 4 show the SEM images of the magnetite and maghemite products, respectively. The character of the nanostructures is inherited during the phase transformation from hematite to magnetite and further to maghemite. The XRD patterns of magnetite and maghemite nanostructures are shown in Figure 4c. All of the reflection peaks can be well assigned to a spinel structure with the characteristic reflections of iron oxide. However, it is hard to identify magnetite and maghemite only on the basis of the ordinary XRD patterns due to the same spinel structure and similar lattice parameters. It is known that the Raman spectrum is a facile and direct tool to differentiate magnetite and maghemite.[26−28] The Raman spectra of the as-prepared products are presented in Figure 4d. For the magnetite, the spectrum exhibits three discernible peaks at 668 cm^{-1} (A_{1g}) and 536 and 308 cm^{-1} (T_{2g}), which is highly consistent with the reported results for megnetite.[28,29] For the maghemite, the modes positioned at 723 (A_{1g}), 665 (A_{1g}), 507 (T_{2g}), 390 (T_{2g}), 345 (E_g), 263, and 193 cm^{-1} appear in the Raman spectrum, which are all well indexed to the characteristic bands of maghemite.[26,30] The Raman spectra firmly confirmed that the nanostructures shown in parts a and b of Figure 4 can be ascribed to pure magnetite and maghemite, respectively.

Figure 5 shows the results of the HRTEM analysis on a single maghemite tube-in-tube nanostructure. It can be seen that the single-crystal nature of the nanostructure is perfectly kept after a reduction and reoxidation process, indicating that the tube-in-tube structure is stable. Generally speaking, the orientational

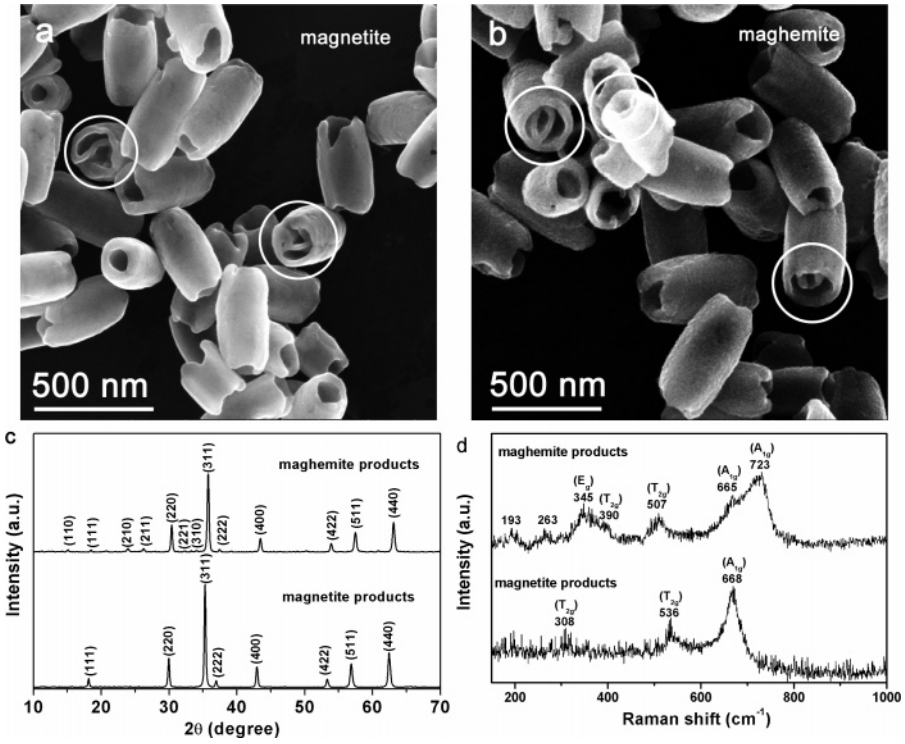

Figure 4. SEM images of the magnetite (a) and maghemite (b) products, XRD patterns (c), and Raman spectra (d). The tube-in-tube nanostructures are marked with circles in (a) and (b).

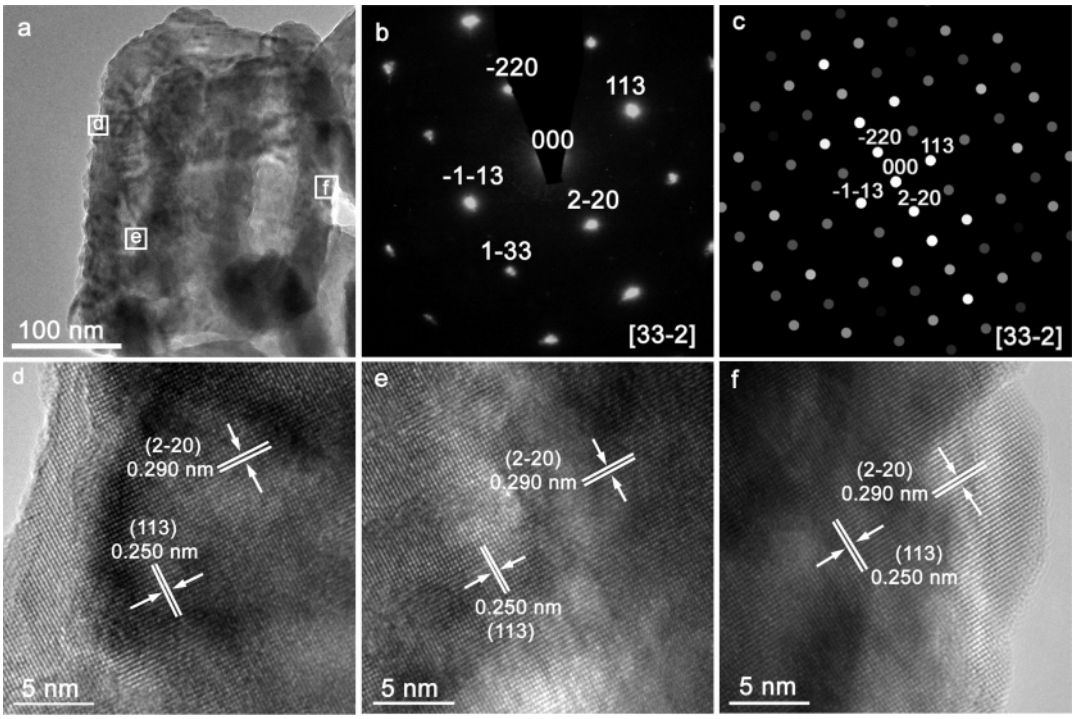

Figure 5. TEM image (a), SAED pattern (b), simulated ED pattern (c), and HRTEM images (d−f) of a single maghemite tube-in-tube nanostructure viewed from the side.

relationship for the phase transformation of α-Fe_2O_3 → Fe_3O_4 → γ-Fe_2O_3 is $[001]_{\alpha-Fe_2O_3}||[111]_{Fe_3O_4}||[111]_{\gamma-Fe_2O_3}$,[31−33] which is called "topotactic transformation". For the maghemite tube-in-tube nanostructure, the longitudinal direction is not a low-index one, which could be confirmed by the SAED pattern (Figure 5b) and the HRTEM images (Figures 5d−f) of the different parts. The ED pattern simulated by JEMS software[34] (Figure 5c) with the electron incidence direction of $[3\,3\,-2]_{\gamma-Fe_2O_3}$ is highly consistent with that in Figure 5b, further confirming the above results. Further study on the orientational relationship for the phase transformation of α-Fe_2O_3 → Fe_3O_4 → γ-Fe_2O_3 is still in progress.

The primary magnetic properties of the magnetite and maghemite nanostructures (as shown in Figure 4a,b) were also investigated. Figure 6 shows the hysteresis loop of the magnetite and maghemite products. The coercive force (H_c) at 300 K is 210 and 170 Oe for the magnetite and maghemite products, respectively. The saturation magnetization (M_s) of the magnetite

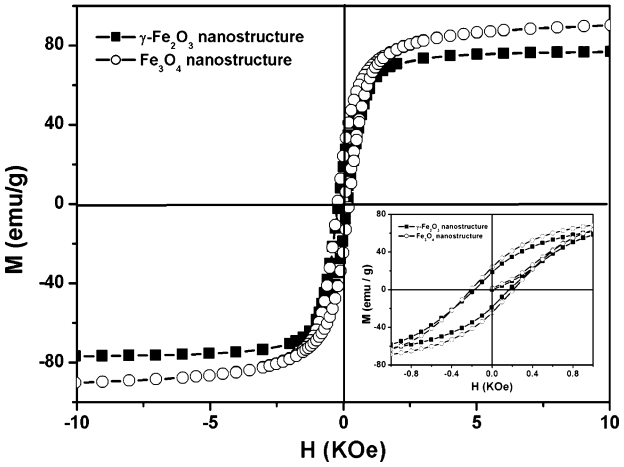

Figure 6. Hysteresis loop of the magnetite and maghemite products shown in parts a and b Figure 4, respectively, at 300 K. Inset: enlargement of the loop.

and maghemite nanostructures is 90 and 77 emu/g, respectively, just a little lower than that of the corresponding bulk values (92 emu/g[35] for Fe_3O_4, 80 emu/g[36] for γ-Fe_2O_3). The temperature dependence of magnetization of the magnetite and maghemite nanostructures was also measured by applying a magnetic field of 10 Oe as ZFC−FC curves (Figure S8, Supporting Information). For magnetite products, there is an apparent magnetic transition around 119 K in its ZFC curve, which corresponds to the Verwey transition originating from a fast electron hopping process between Fe^{3+} and Fe^{2+} ions in the B site of magnetite.[37] The Verwey transition is a special character of magnetite, and this observation further confirms the structure of the product, while for maghemite products, no magnetic transition is observed in its ZFC−FC curves. The hematite, magnetite, and maghemite tube-in-tube nanostructures not only enrich the nanostructures of iron oxides, but also provide new candidates with novel morphology for single-nanomagnet magnetism studies and nanodevices.

Conclusion

We report a facile way to synthesize single-crystal hematite tube-in-tube nanostructures, which were formed with a multisite dissolution process of ellipsoid precursors. This strategy may be useful to achieve other complex single-crystal architectures. With the hematite products as precursors, magnetite and maghemite tube-in-tube nanostructures were also prepared through a reduction or a reduction and reoxidation process. The synthesis of iron oxide tube-in-tube nanostructures not only enriches the iron oxide chemistry, but also could be helpful for constructing complex nanostructures as well as nanodevices.

Acknowledgment. This work was supported by the NSFC (Grant Nos. 20671005, 20221101, and 20423005), MOST (Grant 2006CB601104), and the Founder Foundation of Peking Univeristy.

Supporting Information Available: EDX spectra, SEM, TEM, and HRTEM images, and ZFC and FC curves. This material is available free of charge via the Internet at http://pubs.acs.org.

References and Notes

(1) Iijima, S. *Nature* **1991**, *354*, 56.
(2) Xia, Y. N.; Yang, P. D.; Sun, Y. G.; Wu, Y. Y.; Mayers, B.; Gates, B.; Yin, Y. D.; Kim, F.; Yan, Y. Q. *Adv. Mater*. **2003**, *15*, 353.
(3) Remskar, M. *Adv. Mater.* **2004**, *16*, 1497.
(4) Tenne, R. *Nat. Nanotechnol.* **2006**, *1*, 103.
(5) Zhang, Y.; Suenaga, K.; Colliex, C.; Iijima, S. *Science* **1998**, *281*, 973.
(6) Hu, J. Q.; Bando, Y.; Liu, Z. W. *Adv. Mater*. **2003**, *15*, 1000.
(7) Zhu, Z. P.; Su, D. S.; Weinberg, G.; Schlögl, R. *Nano Lett.* **2004**, *4*, 2255.
(8) Zhu, Z. P.; Su, D. S.; Weinberg, G.; Jentoft, R. E.; Schlögl, R. *Small* **2005**, *1*, 107.
(9) Ozaki, M.; Kratohvil, S.; Matijevic, E. *J. Colloid Interface Sci*. **1984**, *102*, 146.
(10) Sugimoto, T.; Wang, Y. S. *J. Colloid Interface Sci*. **1998**, *207*, 137.
(11) Park, J.; An, K. J.; Hwang, Y. S.; Park, J. G.; Noh, H. J.; Kim, J. Y.; Park, J. H.; Hwang, N. M.; Hyeon, T. *Nat. Mater*. **2004**, *3*, 891.
(12) Jana, N. R.; Chen, Y. F.; Peng, X. G. *Chem. Mater*. **2004**, *16*, 3931.
(13) Li, Z.; Sun, Q.; Gao, M. Y. *Angew. Chem., Int. Ed*. **2005**, *44*, 123.
(14) Wen, X. G.; Wang, S. H.; Ding, Y.; Wang, Z. L.; Yang, S. H. *J. Phys. Chem. B* **2005**, *109*, 215.
(15) Morber, J. R.; Ding, Y.; Haluska, M. S.; Li, Y.; Liu, J. P.; Wang, Z. L.; Snyder, R. L. *J. Phys. Chem. B* **2006**, *110*, 21672.
(16) Chueh, Y. L; Lai, M. W.; Liang, J. Q.; Chou, L. J.; Wang, Z. L. *Adv. Funct. Mater*. **2006**, *16*, 2243.
(17) Liu, Z.; Zhang, D.; Han, S.; Li, C.; Lei, B.; Lu, W.; Fang, J.; Zhou, C. *J. Am. Chem. Soc*. **2005**, *127*, 6.
(18) Chen, J.; Xu, L. N.; Li, W. Y.; Gou, X. L. *Adv. Mater*. **2005**, *17*, 582.
(19) Jia, C. J.; Sun, L. D.; Yan, Z. G.; You, L. P.; Luo, F.; Han, X. D.; Pang, Y. C.; Zhang, Z.; Yan, C. H. *Angew. Chem., Int. Ed.* **2005**, *44*, 4328.
(20) Tartaj, P.; Gonzalez-Carreno, T.; Serna, C. J. *Adv. Mater*. **2004**, *16*, 529.
(21) Cao, M. H.; Liu, T. F.; Gao, S.; Sun, G. B.; Wu, X. L.; Hu, C. W.; Wang, Z. L. *Angew. Chem., Int. Ed.* **2005**, *44*, 4197.
(22) Chen, D. H.; Chen, D. R.; Jiao, X. L.; Zhao, Y. T. *J. Mater. Chem.* **2003**, *13*, 2266.
(23) Raming, T. P.; Winnubst, A. J. A.; van Kats, C. M.; Philipse, A. P. *J. Colloid Interface Sci*. **2002**, *249*, 346.
(24) Zysler, R. D.; Fiorani, D.; Testa, A. M.; Suber, L.; Agostinelli, E.; Godinho, M. *Phys. Rev. B* **2003**, *68*, 212408.
(25) Rath, C.; Sahu, K. K.; Kulkarni, S. D.; Anand, S.; Date, S. K.; Das, R. P.; Mishra, N. C. *Appl. Phys. Lett*. **1999**, *75*, 4171.
(26) Thierry, D.; Persson, D.; I-eygraf C.; Delichère, D.; Joiret, S.; Pallotta, C.; Hugot-Le Goff A. *J. Electrochem. Soc*. **1988**, *135*, 305.
(27) De Faria, D. L. A.; Venancio Silva, S.; De Oliveira, M. T. *J. Raman Spectrosc*. **1997**, *28*, 873.
(28) Pinna, N.; Grancharov, S.; Beato, P.; Bonville, P.; Antonietti, M.; Niederberger, M. *Chem. Mater*. **2005**, *17*, 3044.
(29) Shebanova, O. N.; Lazor, P. *J. Raman Spectrosc.* **2003**, *34*, 845.
(30) Chernyshova, I. V.; Hochella, M. F., Jr.; Madden, A. S. *Phys. Chem. Chem. Phys*. **2007**, *9*, 1736.
(31) Becker, P. P.; Heizmann, J. J.; Baro, R. *J. Appl. Crystallogr*. **1977**, *10*, 77.
(32) Varanda, L, C,; Jafelicci, M.; Tartaj, P.; O'Grady, K.; Gonzalez-Carreno, T.; Morales, M. P.; Munoz, T.; Serna, C. J. *J. Appl. Phys*. **2002**, *92*, 2079.
(33) Morales, M. P.; Pecharroman, C.; Gonzalez-Carreno, T.; Serna, C. J. *J. Solid State Chem.* **1994**, *108*, 158.
(34) Stadelmann, P. *JEMS, Electron Microscopy Software*, Java Version 3.0512W2006; CIME-EPFL: Laussane, Switzerland.
(35) Smit, J.; Wijn, H. P. *Ferrie*; Wiley: New York, 1959; p 369.
(36) Dutta, P.; Manivannan, A.; Seehra, M. S.; Shah, N.; Huffman, G. P. *Phys. Rev. B* **2004**, *70*, 174428.
(37) Verwey, E. J. W. *Nature* **1939**, *144*, 327.